ELSEVIER

International Journal of Heat and Fluid Flow 21 (2000) 412–419

International Journal of HEAT AND FLUID FLOW

www.elsevier.com/locate/ijhff

Numerical prediction of air core diameter, coefficient of discharge and spray cone angle of a swirl spray pressure nozzle

A. Datta [a,*], S.K. Som [b]

[a] Department of Power Plant Engineering, Jadavpur University, 2nd Campus, Salt Lake, Calcutta 700091, India
[b] Department of Mechanical Engineering, Indian Institute of Technology, Kharagpur 721302, India

Received 20 April 1999; accepted 9 November 1999

Abstract

Theoretical predictions of air core diameter, coefficient of discharge and spray cone angle of a swirl spray pressure nozzle have been made from numerical computations of flow within the nozzle. The diameter of central air core that stabilizes inside the nozzle has been predicted from a hydrodynamic situation that yields the minimum resistance to the liquid flow in the nozzle at given operating conditions. The coefficient of discharge and spray cone angle have been evaluated from the distributions of the different velocity components of liquid flow at the nozzle orifice. It has been observed that the coefficient of discharge C_d decreases, while the air core diameter d_a and spray cone angle ψ increase with the increase in nozzle flow in its lower range. However, all these parameters C_d, d_a and ψ finally become independent of nozzle flow. Predicted values of d_a, C_d and ψ for different geometrical dimensions of the nozzle have been compared with the empirical data available in the literature.

Keywords: Atomize; Swirl; Air core; Coefficient of discharge; Spray cone angle

1. Introduction

The importance of a swirl spray pressure nozzle lies in its widespread industrial applications in combustion, evaporation, drying, humidification, cooling, air-conditioning, sprinkling etc. A unified design approach of nozzle in these fields requires the interrelations between different performance characteristics of the nozzle with pertinent input parameters such as, liquid properties, injection conditions and nozzle geometry. This needs a physical understanding of the flow inside the nozzle and mechanism of spray formation outside the nozzle. The simplest form of a pressure swirl nozzle is the one known as simplex nozzle as shown in Fig. 1a. Liquid is fed into the swirl chamber through tangential ports and is finally discharged from an outlet orifice of the nozzle. Due to the tangential entry, an air-cored vortex flow of liquid takes place in the nozzle (Fig. 1b) and the liquid comes out of the orifice in the form of a thin film which, due to its inherent hydrodynamic instability, disintegrates into ligaments and then drops in the form of a well defined hollow cone spray.

The formation of a central air core is the most important picture of the flow in a simplex nozzle. The size of the air core determines the effective flow area at the discharge orifice and thus controls the coefficient of discharge, which is one of the important performance parameter of the nozzle. Another important performance parameter is the spray cone angle that determines the coverage and dispersion of spray in the surrounding ambiance. Despite the geometrical simplicity of the simplex nozzle, the situation of turbulent swirling flow with a central air core in the nozzle is highly complex. Most of the works available in the literature in this area are empirical or semi-empirical in nature. Taylor (1948) gave the most valid and pioneering theoretical treatment for potential flow in a swirl nozzle and predicted that the air core diameter and spray cone angle were inverse functions, while the coefficient of discharge is a direct function of a single dimensionless geometrical parameter defined as nozzle constant ($K_1 = A_p/d_s d_o$), where A_p was the area of tangential entry ports and d_s and d_o were the diameters of the swirl chamber and discharge orifice, respectively. But his theory referred to a simplified cylindrical swirl chamber and could not explain the dependence of performance parameters on nozzle flow as occurs in practice. However, in a subsequent work, Taylor (1950) provided a theoretical treatment for the growth of boundary layer for a laminar swirling flow in a convergent duct. The classical works in the field include those of Binnie and Harris (1950), Giffen and Massey (1950), Tate and Marshall (1953), Binnie (1955), Binnie and Teare (1956) and Binnie et al. (1957). Those works mostly referred to experimental investigations of swirling liquid flow through straight and convergent ducts. The recent developments in the field of simplex type swirl nozzle are mainly due to Kutty et al. (1978), Som and Mukherjee (1980), Jones (1982), Rizk and Lefebvre (1985a,b), Suyari and Lefebvre (1986), Wang and

* Corresponding author.
E-mail address: jupower@cal.vsnl.net.in (A. Datta).

0142-727X/00/$ - see front matter
PII: S0142-727X(00)00003-5

Notation

A_0	cross-sectional area of discharge plane
A_p	cross-sectional area of the injection ports
C_d	coefficient of discharge
c_μ, $c_{1\varepsilon}$, $c_{2\varepsilon}$	empirical constants of k–ε equations
d	diameter
I	turbulent intensity
L	turbulent length scale
l	length
p	pressure
Q	liquid flow rate
r	radial position
r_a	radius of air core
r_o	radius of exit orifice
r_s	radius of the swirl chamber
r_z	radius of the nozzle at any axial location z
t	time
t_f	liquid film thickness
V	average velocity at the discharge plane
v	velocity
z	axial co-ordinate
α	half cone angle of the swirl chamber
ε	turbulent kinetic energy dissipation rate
μ	viscosity
ν	kinematic viscosity
ν_t	turbulent viscosity
ρ	density
ψ	spray cone angle
σ_k, σ_ε	empirical constants of k–ε equations

Superscript

a	air phase
l	liquid phase

Subscript

a	air core
e	exit plane
in	inlet plane
o	orifice
r	radial direction
s	swirl chamber
z	axial direction
θ	azimuthal direction

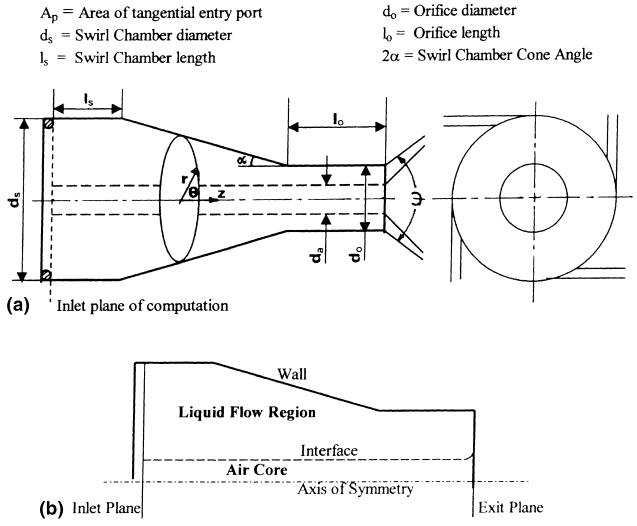

Fig. 1. (a) Geometry and nomenclature of a simplex type swirl spray pressure nozzle. (b) Physical model of the problem.

Lefebvre (1987) and Chen et al. (1992). All these works have brought about an understanding of the swirling flow inside the nozzle and attempt in evaluating the liquid film thickness at the discharge, flow number and spray cone angle of the nozzle either from empirical studies or from a simplified theory. The recent work of Rizk and Lefebvre (1985a) has referred to a theoretical prediction of liquid film thickness at the discharge orifice of a simplex nozzle. However, the theory proposed by them was based on the force balance of a fluid element in a laminar flow along with the consideration of constant pressure gradient across the liquid film. A full scale numerical approach for the solution of a two phase turbulent swirling flow in a simplex nozzle in predicting air core diameter and finally the coefficient of discharge and spray cone angle as functions of nozzle flow and nozzle geometry is hardly found in the literature till today. An attempt in this direction has therefore been made in the present paper.

2. Theoretical formulation

The theoretical analysis refers to a simplex nozzle as shown in Fig. 1a. The corresponding physical model is shown in Fig. 1b. The flow inside the nozzle becomes axi-symmetric provided the entry of liquid is made through a number of tangential ports or slots placed symmetrically around the periphery at the base of the swirl chamber. The flow in the liquid phase is turbulent due to the high average velocity, however, within the air core the flow is considered to be laminar due to the higher kinematic viscosity of air compared to the liquid.

Standard k–ε model has been adopted for the computation of turbulent flow in the liquid phase. This is despite the fact that many researchers observe some shortcomings in the ability of the standard k–ε model in predicting the swirling flow results, at least quantitatively. However, since there is no conclusive information available in the literature regarding the accurate adaptability of a suitable modification of the k–ε model for a two phase confined swirling flow and the models like ASM and RSM are either too complex or equally poor in predicting the strong swirling flow, standard k–ε model has been considered for the solution in the present work.

Conservation equations for the axi-symmetric flows in both the liquid and air phases are written in the cylindrical co-ordinate system as follows.

2.1. Governing equations

Continuity:

Liquid phase:

$$\frac{\partial v_r^l}{\partial r}+\frac{v_r^l}{r}+\frac{\partial v_z^l}{\partial z}=0. \tag{1a}$$

Air phase:

$$\frac{\partial v_r^a}{\partial r}+\frac{v_r^a}{r}+\frac{\partial v_z^a}{\partial z}=0. \tag{1b}$$

r-Momentum:

Liquid phase:

$$\frac{\partial v_r^{\mathrm{l}}}{\partial t}+\frac{\partial}{\partial r}\left(v_r^{\mathrm{l}^2}\right)+\frac{\partial}{\partial z}\left(v_z^{\mathrm{l}}v_r^{\mathrm{l}}\right)+\frac{v_r^{\mathrm{l}^2}-v_\theta^{\mathrm{l}^2}}{r} =-\frac{1}{\rho^{\mathrm{l}}}\frac{\partial p^{\mathrm{l}}}{\partial r}+2\frac{\partial}{\partial r}\left(\nu_{\mathrm{eff}}^{\mathrm{l}}\frac{\partial v_r^{\mathrm{l}}}{\partial r}\right)+\frac{2}{r}\nu_{\mathrm{eff}}^{\mathrm{l}}\left(\frac{\partial v_r^{\mathrm{l}}}{\partial r}-\frac{v_r^{\mathrm{l}}}{r}\right) +\frac{\partial}{\partial z}\left\{\nu_{\mathrm{eff}}^{\mathrm{l}}\left(\frac{\partial v_z^{\mathrm{l}}}{\partial r}+\frac{\partial v_r^{\mathrm{l}}}{\partial z}\right)\right\}. \tag{2a}$$

Air phase:

$$\frac{\partial v_r^{\mathrm{a}}}{\partial t}+\frac{\partial}{\partial r}\left(v_r^{\mathrm{a}^2}\right)+\frac{\partial}{\partial z}\left(v_z^{\mathrm{a}}v_r^{\mathrm{a}}\right)+\frac{v_r^{\mathrm{a}^2}-v_\theta^{\mathrm{a}^2}}{r} =-\frac{1}{\rho^{\mathrm{a}}}\frac{\partial p^{\mathrm{a}}}{\partial r}+\nu^{\mathrm{a}}\left(\frac{\partial^2 v_r^{\mathrm{a}}}{\partial r^2}+\frac{1}{r}\frac{\partial v_r^{\mathrm{a}}}{\partial r}-\frac{v_r^{\mathrm{a}}}{r}+\frac{\partial^2 v_r^{\mathrm{a}}}{\partial z^2}\right). \tag{2b}$$

z-Momentum:

Liquid phase:

$$\frac{\partial v_z^{\mathrm{l}}}{\partial t}+\frac{\partial}{\partial r}\left(v_r^{\mathrm{l}}v_z^{\mathrm{l}}\right)+\frac{\partial}{\partial z}\left(v_z^{\mathrm{l}^2}\right)+\frac{2v_r^{\mathrm{l}}v_z^{\mathrm{l}}}{r} =-\frac{1}{\rho^{\mathrm{a}}}\frac{\partial p^{\mathrm{l}}}{\partial z}+\frac{1}{r}\frac{\partial}{\partial r}\left\{r\nu_{\mathrm{eff}}^{\mathrm{l}}\left(\frac{\partial v_z^{\mathrm{l}}}{\partial r}+\frac{\partial v_r^{\mathrm{l}}}{\partial z}\right)\right\} +2\frac{\partial}{\partial z}\left\{\nu_{\mathrm{eff}}^{\mathrm{l}}\frac{\partial v_z^{\mathrm{l}}}{\partial z}\right\}. \tag{3a}$$

Air phase:

$$\frac{\partial v_z^{\mathrm{a}}}{\partial t}+\frac{\partial}{\partial r}\left(v_r^{\mathrm{a}}v_z^{\mathrm{a}}\right)+\frac{\partial}{\partial z}\left(v_z^{\mathrm{a}^2}\right)+\frac{v_r^{\mathrm{a}}v_z^{\mathrm{a}}}{r} =-\frac{1}{\rho^{\mathrm{a}}}\frac{\partial p^{\mathrm{a}}}{\partial z}+\nu^{\mathrm{a}}\left(\frac{\partial^2 v_z^{\mathrm{a}}}{\partial r^2}+\frac{1}{r}\frac{\partial v_z^{\mathrm{a}}}{\partial r}+\frac{\partial^2 v_z^{\mathrm{a}}}{\partial z^2}\right). \tag{3b}$$

θ-Momentum:

Liquid phase:

$$\frac{\partial v_\theta^{\mathrm{l}}}{\partial t}+\frac{\partial}{\partial r}\left(v_r^{\mathrm{l}}v_\theta^{\mathrm{l}}\right)+\frac{\partial}{\partial z}\left(v_z^{\mathrm{l}}v_\theta^{\mathrm{l}}\right)+\frac{2v_r^{\mathrm{l}}v_\theta^{\mathrm{l}}}{r} =\frac{1}{r^2}\frac{\partial}{\partial r}\left\{r^2\nu_{\mathrm{eff}}^{\mathrm{l}}\left(\frac{\partial v_\theta^{\mathrm{l}}}{\partial r}-\frac{v_\theta^{\mathrm{l}}}{r}\right)\right\}+\frac{\partial}{\partial z}\left\{\nu_{\mathrm{eff}}^{\mathrm{l}}\frac{\partial v_\theta^{\mathrm{l}}}{\partial z}\right\}. \tag{4a}$$

Air phase:

$$\frac{\partial v_\theta^{\mathrm{a}}}{\partial t}+\frac{\partial}{\partial r}\left(v_r^{\mathrm{a}}v_\theta^{\mathrm{a}}\right)+\frac{\partial}{\partial z}\left(v_z^{\mathrm{a}}v_\theta^{\mathrm{a}}\right)+\frac{2v_r^{\mathrm{a}}v_\theta^{\mathrm{a}}}{r} =\nu^{\mathrm{a}}\left(\frac{\partial^2 v_\theta^{\mathrm{a}}}{\partial r^2}+\frac{1}{r}\frac{\partial v_\theta^{\mathrm{a}}}{\partial r}-\frac{v_\theta^{\mathrm{a}}}{r^2}+\frac{\partial^2 v_\theta^{\mathrm{a}}}{\partial z^2}\right) \tag{4b}$$

Turbulent kinetic energy (*liquid phase*):

$$\frac{\partial k}{\partial t}+\frac{\partial}{\partial r}\left(v_r^{\mathrm{l}}k\right)+\frac{\partial}{\partial z}\left(v_z^{\mathrm{l}}k\right)+\frac{v_r^{\mathrm{l}}k}{r} =\frac{1}{r}\frac{\partial}{\partial r}\left(r\frac{\nu_t^{\mathrm{l}}}{\sigma_k}\frac{\partial k}{\partial r}\right)+\frac{\partial}{\partial z}\left(\frac{\nu_t^{\mathrm{l}}}{\sigma_k}\frac{\partial k}{\partial z}\right) +\nu_t^{\mathrm{l}}\left[2\left\{\left(\frac{\partial v_r^{\mathrm{l}}}{\partial r}\right)^2+\left(\frac{v_r^{\mathrm{l}}}{r}\right)^2+\left(\frac{\partial v_z^{\mathrm{l}}}{\partial z}\right)^2\right\} +\left(\frac{\partial v_\theta^{\mathrm{l}}}{\partial r}-\frac{v_\theta^{\mathrm{l}}}{r}\right)^2+\left(\frac{\partial v_r^{\mathrm{l}}}{\partial z}+\frac{\partial v_z^{\mathrm{l}}}{\partial r}\right)^2+\left(\frac{\partial v_\theta^{\mathrm{l}}}{\partial z}\right)^2\right]-\varepsilon. \tag{5}$$

Turbulent kinetic energy dissipation rate (*liquid phase*):

$$\frac{\partial \varepsilon}{\partial t}+\frac{\partial}{\partial r}\left(v_r^{\mathrm{l}}\varepsilon\right)+\frac{\partial}{\partial z}\left(v_z^{\mathrm{l}}\varepsilon\right)+\frac{v_r^{\mathrm{l}}\varepsilon}{r} =\frac{1}{r}\frac{\partial}{\partial r}\left(r\frac{\nu_t^{\mathrm{l}}}{\sigma_\varepsilon}\frac{\partial \varepsilon}{\partial r}\right)+\frac{\partial}{\partial z}\left(\frac{\nu_t^{\mathrm{l}}}{\sigma_\varepsilon}\frac{\partial \varepsilon}{\partial z}\right) +c_{1\varepsilon}\frac{\varepsilon}{k}\nu_t^{\mathrm{l}}\left[2\left\{\left(\frac{\partial v_r^{\mathrm{l}}}{\partial r}\right)^2+\left(\frac{v_r^{\mathrm{l}}}{r}\right)^2+\left(\frac{\partial v_z^{\mathrm{l}}}{\partial z}\right)^2\right\} +\left(\frac{\partial v_\theta^{\mathrm{l}}}{\partial r}-\frac{v_\theta^{\mathrm{l}}}{r}\right)^2+\left(\frac{\partial v_r^{\mathrm{l}}}{\partial z}+\frac{\partial v_z^{\mathrm{l}}}{\partial r}\right)^2+\left(\frac{\partial v_\theta^{\mathrm{l}}}{\partial z}\right)^2\right]-c_{2\varepsilon}\frac{\varepsilon^2}{k}. \tag{6}$$

The empirical constants for Eqs. (5) and (6) are taken as follows:

$$\sigma_k=1.0,\quad \sigma_\varepsilon=1.3,\quad c_{1\varepsilon}=1.44,\quad c_{2\varepsilon}=1.92.$$

2.2. Air core diameter

Experimental observations (Giffen and Massey, 1950; Som and Mukherjee, 1980) have established that beyond a certain injection pressure the stable air core inside the nozzle is cylindrical with a little enlargement near the exit plane as shown (by the dashed line) in Fig. 1b. The expansion may be due to the change over from the confined to the unconfined nature of the flow with tangential velocity. The liquid–air interface is a free surface where the normal deviatoric stresses and pressures in both the phases balance the surface tension. However, the present work assumes the air core to be entirely cylindrical and determines the air core diameter from the principle of least resistance path followed by any naturally stable flow as follows.

The resistance to a flow is manifested by the pressure drop across the flow. In consideration of the radial pressure gradient due to tangential velocity component of the liquid at the discharge plane, the total pressure drop (Δp) in a swirl nozzle can be written as,

$$\Delta p=\Delta p_{\mathrm{w}}+\Delta p_r, \tag{7}$$

where Δp_{w} is the pressure drop along the nozzle wall due to friction and Δp_r is the pressure drop in the radial direction due to tangential component of liquid motion at the discharge plane. In the present numerical experiments, values of Δp have been computed for different values of air core diameter imposed arbitrarily in the nozzle flow for a given value of flow rate and given geometrical dimensions of the nozzle. This has been done to generate the relationship of pressure drop Δp with the diameter of the imposed air core for a given flow in a nozzle of fixed dimension (Fig. 2). It is found that an increase in air core diameter upto a certain value does not make any change in the total pressure drop in the nozzle because of the counterbalancing effects of Δp_{w} and Δp_r. However, beyond a critical value of air core diameter, the pressure drop Δp increases with any further increase in air core diameter. It is expected that once the air begins to fill in from the outside creating the air core, the ingress continues and the core grows on developing till the critical value of air core diameter is reached when the flow tends to suffer from more resistance as depicted by the onset of an increasing trend in total pressure drop Δp with air core diameter d_{a}. The present theory proposes the critical air core diameter as the stable air core diameter for the specified operating parameters.

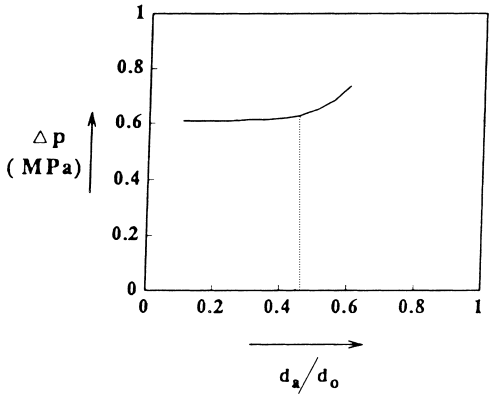

Fig. 2. Variation of total pressure drop (Δp) with d_a/d_o. $Q = 5 \times 10^{-5}$ m^3/s, $d_s = 8$ mm, $d_o = 2$ mm, $l_s = 1$ mm, $l_o = 4$ mm, $2\alpha = 41^\circ$.

2.3. Boundary conditions

Eqs. (1)–(6) are solved in the liquid and air phases with the air core diameter determined in the manner explained above. The boundary conditions, adopted for the solution of the conservation equations, are as follows:

Inlet plane:

$$v_z^1 = u_o, \quad v_r^1 = 0, \quad v_\theta^1 = \frac{Qr_s}{A_p r}, \quad k = k_{in} = \frac{3}{2} I_{in}^2 u_o^2,$$
$$\varepsilon = \varepsilon_{in} = \frac{k_{in}^{1.5}}{L_{in}}, \quad v_z^a = v_r^a = v_\theta^a = 0. \tag{8a}$$

In the liquid phase, at the inlet, axial velocity distribution is considered to be in the plug flow mode with a tangential velocity distribution maintaining a free vortex. The turbulent intensity and scale are specified at the inlet plane as $I_{in} = 0.1$ and $L_{in} = 0.005 d_s$. In the air phase no flow is considered at the inlet plane of computation.

Exit plane:

$$\frac{\partial^2 v_z^1}{\partial z^2} = \frac{\partial^2 v_r^1}{\partial z^2} = \frac{\partial^2 v_\theta^1}{\partial z^2} = \frac{\partial^2 k}{\partial z^2} = \frac{\partial^2 \varepsilon}{\partial z^2} = 0, \ \frac{\partial^2 v_z^a}{\partial z^2} = \frac{\partial^2 v_r^a}{\partial z^2} = \frac{\partial^2 v_\theta^a}{\partial z^2} = 0. \tag{8b}$$

At the exit plane the second axial derivative of the variables are equated to zero to ensure smooth transition of flow at the nozzle exit.

Liquid–air interface:

$$v_z^1 = v_z^a, v_r^1 = v_r^a, v_\theta^1 = v_\theta^a, \quad \tau_{rz}^1 = \tau_{rz}^a, \tau_{r\theta}^1 = \tau_{r\theta}^a,$$
logarithmic law of the wall. (8c)

At the liquid–air interface the continuity of velocities and tangential stresses between the two phases are considered. Logarithmic law of the wall, as applied for the solid surface, is taken as no separate wall law is available in the literature for the liquid–air interface.

Axis of symmetry:

$$\frac{\partial v_z^a}{\partial r} = v_r^a = v_\theta^a = 0. \tag{8d}$$

Outer wall:

$$v_z^1 = v_r^1 = v_\theta^1 = 0, \quad \text{logarithmic law of wall.} \tag{8e}$$

The boundary condition at the outer wall is considered satisfying the no slip condition.

2.4. Coefficient of discharge and spray cone angle

The coefficient of discharge and spray cone angle are determined from the following expressions as,

$$C_d = \frac{Q}{A_0 \left(\frac{2\Delta p}{\rho^1}\right)^{1/2}}, \tag{9a}$$

$$\psi = 2 \cos^{-1}\left(\frac{V_z^1}{\sqrt{\left(V_z^{l2} + V_r^{l2} + V_\theta^{l2}\right)}}\right). \tag{9b}$$

The average axial, tangential and radial components of liquid velocities at the nozzle orifice are determined as,

$$V_z^1 = \frac{4Q}{\pi\left(d_o^2 - d_a^2\right)}, \tag{10a}$$

$$V_r^1 = \frac{\int_{r_a}^{r_o} r v_{z_e}^1 v_{r_e}^1 \, dr}{\int_{r_a}^{r_o} r v_{z_e}^1 \, dr}, \tag{10b}$$

$$V_\theta^1 = \frac{\int_{r_a}^{r_o} r v_{z_e}^1 v_{\theta_e}^1 \, dr}{\int_{r_a}^{r_o} r v_{z_e}^1 \, dr}. \tag{10c}$$

3. Method of solution

Eqs. (1)–(6) were solved simultaneously in both the liquid and air phases satisfying the respective boundary conditions by an explicit finite difference computing technique developed by Hirt and Cook (1972) following the original MAC (marker and Cell) method due to Harlow and Welch (1965). The steady state solution of flow was achieved by advancing the equations in time till the temporal derivatives of all the variables fall below a pre-assigned small quantity δ.

The space derivatives of the diffusion terms were discretised by the central differencing scheme, while the advection terms were discretised by a hybrid differencing scheme based on the local Peclet number (Pe) associated with the cell. A variable sized adaptive grid system was considered with clustered cells near the inlet, wall and interface. In the convergent section of the nozzle the grids were arranged maintaining a rectangular castellation. The variations in the size of the grids were made uniformly. For different sets of experiments, different numbers of cells in either z- or r-directions were chosen. However, in all the cases it was checked that further refinement of the cells did not change the local velocity components by more that 2%. The choice of time increment Δt was made to ensure stability in the computation in accordance with criteria of cell transit time of fluid due to convection and diffusion, respectively. Often a more stringent restriction was required to have a converged solution and was fixed by trial and error in the computation.

4. Results and discussion

The flow fields in both the liquid and air phases in a nozzle for two different flow rates are shown in Figs. 3a and 3b. The interesting feature in the liquid flow is the formation of two recirculating zones, one adjacent to the air core and the other near the wall, at the upstream part of the nozzle. The recirculation zones are the results of the typical swirl entry of liquid considered in the present problem (Figs. 1a and 1b). The radial distribution of axial and tangential velocities of liquid at

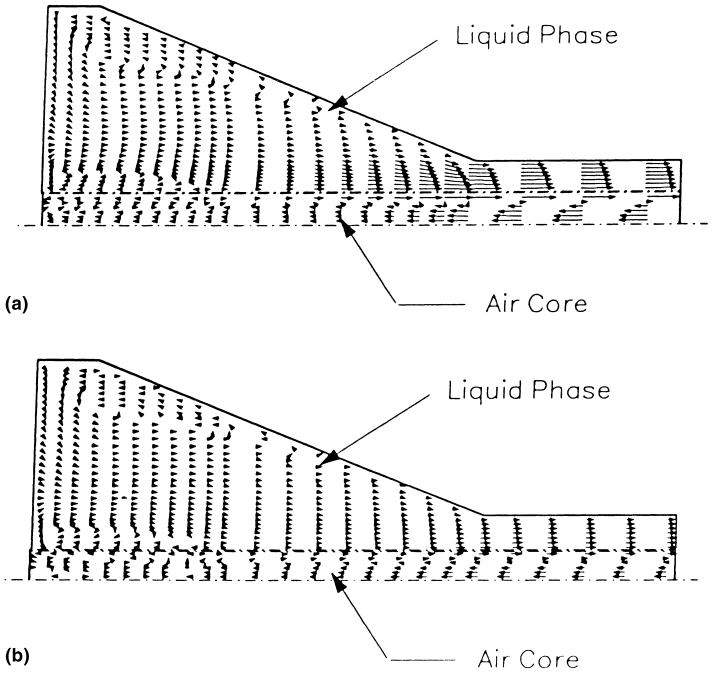

Fig. 3. Velocity vectors inside a simplex type swirl spray pressure nozzle. $d_s = 8$ mm, $d_o = 2$ mm, $l_s = 1$ mm, $2\alpha = 41°$, $l_o = 4$ mm. (a) $Q = 5 \times 10^{-5}$ m^3/s; (b) $Q = 1.25 \times 10^{-5}$ m^3/s.

different axial locations of the nozzle are shown in Figs. 4a and 4b. It is observed that the radial distribution of tangential velocity component changes from a purely vortex one (as assumed in the present problem) at the inlet to a forced vortex type at the outlet. In the upstream part of the nozzle near the inlet, the tangential component of velocity is relatively higher than the axial one and remains almost constant in a region close to the wall extending to a radial location near the axis and then follows a decreasing trend with a decrease in the radius (Figs. 4a[i] and b[i]). In the downstream part of the converging portion of the nozzle (Figs. 4a[ii] and b[ii]), the tangential velocity decreases continuously from the wall to the liquid–air interface. However, the magnitude of the tangential component of velocity is still higher than that of the axial component at all radial locations. In the straight orifice part of the nozzle (Figs. 4a[iii] and b[iii]), the tangential component of velocity becomes smaller in magnitude as compared to that of the axial one and shows almost a forced vortex type distribution with the radial location.

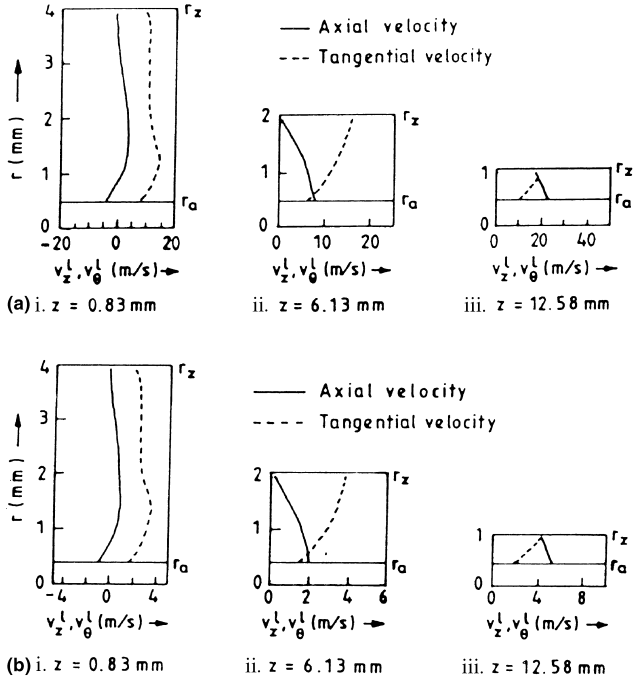

Fig. 4. Axial and tangential velocity distributions of liquid at specified axial locations in a simplex type swirl spray pressure nozzle. $d_s = 8$ mm, $d_o = 2$ mm, $l_s = 1$ mm, $2\alpha = 41°$, $l_o = 4$ mm. (a) $Q = 5 \times 10^{-5}$ m^3/s; (b) $Q = 1.25 \times 10^{-5}$ m^3/s.

The flow field in the air core (Figs. 3a and b), as induced by the liquid motion, depicts an entire recirculation zone in the downstream part of the air core with back flow near the axis and forward flow adjacent to the liquid–air interface, while the upstream part of the air core remains almost stagnant. The length of recirculation zone in the air core increases with an increase in the liquid flow rate through the nozzle.

4.1. Influence of nozzle flow on air core diameter, coefficient of discharge and spray cone angle

It is observed from Fig. 5 that with an increase in the nozzle flow rate, Q, at its lower range, there occurs a sharp increase in the air core diameter, d_a, and spray cone angle, ψ, but a sharp decrease in the coefficient of discharge, C_d. However, all these parameters d_a, ψ and C_d finally become almost independent of the flow rate Q at its higher range. These typical variations can be explained by the physical phenomena as follows.

The formation of a central air core in a simplex nozzle is the consequence of a reduction in pressure near the nozzle axis because of the swirling flow of liquid inside it. Due to the formation of a central air core and existence of high tangential velocity at the nozzle orifice, the coefficient of discharge of a

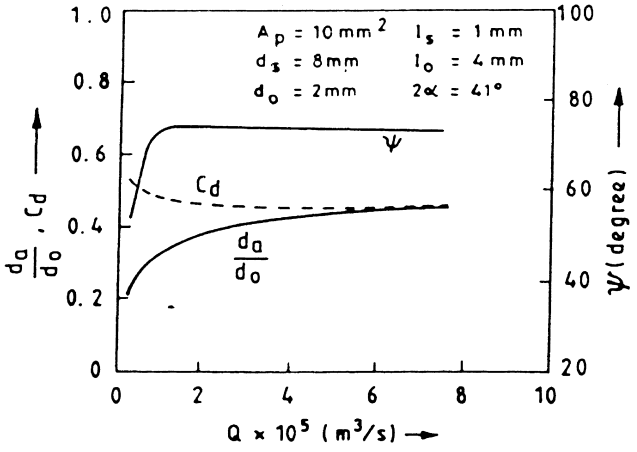

Fig. 5. Variation of air core diameter, coefficient of discharge and spray cone angle with liquid flow rate in the nozzle. $d_s = 8$ mm, $d_o = 2$ mm, $l_s = 1$ mm, $2\alpha = 41°$, $l_o = 4$ mm.

swirl nozzle is low, while its spray cone angle is high. Therefore, the size of the air core and the values of coefficient of discharge and spray cone angle are the index of strength of the swirling motion inside the nozzle. The higher is the swirling strength, higher is the air core diameter or spray cone angle and lower is the coefficient of discharge. An increase in flow rate is accompanied by an increase in the tangential velocity of injection to the nozzle. This causes counterweighing effects on the strength of swirling motion inside the nozzle by increasing both the swirling strength at inlet and its subsequent decay due to frictional effect in the nozzle. In the lower range of the flow rate, Q, the increase in swirl predominates the adverse effect of frictional resistance, while at higher values of Q, the two effects counterbalance each other and result in almost constant values of d_a, ψ and C_d.

4.2. Influence of nozzle geometry on air core diameter, coefficient of discharge and spray cone angle

It is found that an increase in either the orifice diameter or swirl chamber cone angle, or a decrease in the area of inlet tangential ports increases the air core diameter (Tables 1a–d) and spray cone angle (Tables 2a–d) while decreases the coefficient of discharge (Tables 2a–d) and vice versa. The length of the orifice has no influence on these parameters. These trends of variations can be attributed to the fact that an increase in either orifice diameter or swirl chamber cone angle reduces the resistance offered by the nozzle to the swirling motion of liquid inside it, while a decrease in inlet port area, for a given flow rate, increases the strength of swirling motion by increasing the tangential velocity of injection to the nozzle.

The experimental results of Suyari and Lefebvre (1986) and the semi-empirical equation of Rizk and Lefebvre (1985a), based on the experimental results of Kutty et al. (1978), for liquid film thickness at the discharge orifice have been

Table 1
Variation of air core diameter with the geometrical dimensions of the swirl spray pressure nozzle

Orifice diameter (d_o) (mm)	Prediction from the present model (d_a/d_o)	Empirical results from literature; $d_a/d_o = 1 - 2t_f/d_o$		
		Taylor's inviscid theory (1948)	Rizk and Lefebvre (1985a)	Suyari and Lefebvre (1986)
(a) Influence of orifice diameter (d_o) ($Q = 5 \times 10^{-5}$ m^3/s, $A_p = 10$ mm^2, $d_s = 8$ mm, $l_a = 1$ mm, $l_o = 4$ mm, $2\alpha = 41°$)				
1.0	0.35	0.529	0.584	0.692
1.5	0.4	0.591	0.577	0.688
2.0	0.45	0.632	0.59	0.697
Swirl chamber cone angle (2α) (degree)	Prediction from the present model (d_a/d_o)	Empirical results from literature; $d_a/d_o = 1 - 2t_f/d_o$		
		Taylor's inviscid theory (1948)	Rizk and Lefebvre (1985a)	Suyari and Lefebvre (1986)
(b) Influence of swirl chamber cone angle (2α) ($Q = 5 \times 10^{-5}$ m^3/s, $A_p = 10$ mm^2, $d_s = 8$ mm, $l_s = 1$ mm, $l_o = 4$ mm, $d_o = 41°$)				
21	0.4	0.632	0.567	0.68
41	0.45	0.632	0.59	0.697
53	0.47	0.632	0.596	0.702
Orifice length (l_o) (mm)	Prediction from the present model (d_a/d_o)	Empirical results from literature; $d_a/d_o = 1 - 2t_f/d_o$		
		Taylor's inviscid theory (1948)	Rizk and Lefebvre (1985a)	Suyari and Lefebvre (1986)
(c) Influence of orifice length (l_o) ($Q = 5 \times 10^{-5}$ m^3/s, $A_p = 10$ mm^2, $d_s = 8$ mm, $l_s = 1$ mm, $2\alpha = 41°$, $d_o = 2$ mm)				
3.0	0.45	0.632	0.589	0.697
4.0	0.45	0.632	0.59	0.697
6.0	0.45	0.632	0.59	0.697
Injection port area (A_p) (mm^2)	Prediction from the present model (d_a/d_o)	Empirical results from literature; $d_a/d_o = 1 - 2t_f/d_o$		
		Taylor's inviscid theory (1948)	Rizk and Lefebvre (1985a)	Suyari and Lefebvre (1986)
(d) Influence of injection port area (A_p) ($Q = 5 \times 10^{-5}$ m^3/s, $d_s = 8$ mm, $l_s = 1$ mm, $2\alpha = 41°$, $l_o = 4$ mm, $d_o = 2$ mm)				
10	0.45	0.632	0.59	0.697
16	0.38	0.565	0.548	0.666

Table 2
Variation of coefficient of discharge (C_d) and spray cone angle (ψ) with the geometrical dimensions of the simplex nozzle

Orifice diameter d_o (mm)	C_d from present model	Empirical value of C_d from literature		ψ from present model	Empirical value of ψ from literature
		Rizk and Lefebvre (1985a)	Jones (1982)		Rizk and Lefebvre (1985b)
(a) Influence of orifice diameter (d_o) ($Q = 5 \times 10^{-5}$ m^3/s, $A_p = 10$ mm^2, $d_s = 8$ mm, $l_s = 1$ mm, $l_o = 4$ mm, $2\alpha = 41°$)					
1.0	0.656	0.658	0.625	38.78	67.23
1.5	0.548	0.484	0.468	56.89	68.03
2.0	0.448	0.39	0.382	73.51	69.6
Swirl chamber cone angle (2α)	C_d from present model	Empirical value of C_d from literature		ψ from present model	Empirical value of ψ from literature
		Rizk and Lefebvre (1985a)	Jones (1982)		Rizk and Lefebvre (1985b)
(b) Influence of swirl chamber cone angle (2α) ($Q = 5 \times 10^{-5}$ m^3/s, $A_p = 10$ mm^2, $d_s = 8$ mm, $l_s = 1$ mm, $l_o = 4$ mm, $d_o = 2$ mm)					
21	0.499	0.39	0.396	68.84	68.02
41	0.448	0.39	0.382	73.51	69.6
53	0.434	0.39	0.376	75.78	70.15
Orifice length l_o (mm)	C_d from present model	Empirical value of C_d from literature		ψ from present model	Empirical value of ψ from literature
		Rizk and Lefebvre (1985a)	Jones (1982)		Rizk and Lefebvre (1985b)
(c) Influence of orifice length (l_o) ($Q = 5 \times 10^{-5}$ m^3/s, $A_p = 10$ mm^2, $d_s = 8$ mm, $l_s = 1$ mm, $2\alpha = 41°$, $d_o = 2$ mm)					
3.0	0.448	0.39	0.385	74.30	69.63
4.0	0.448	0.39	0.382	73.51	69.6
6.0	0.447	0.39	0.378	72.05	69.7
Injection port area A_p (mm^2)	C_d from present model	Empirical value of C_d from literature		ψ from present model	Empirical value of ψ from literature
		Rizk and Lefebvre (1985a)	Jones (1982)		Rizk and Lefebvre (1985b)
(d) Influence of injection port area (A_p) ($Q = 5 \times 10^{-5}$ m^3/s, $d_s = 8$ mm, $l_s = 1$ mm, $2\alpha = 41°$, $l_o = 4$ mm, $d_o = 2$ mm					
10	0.448	0.39	0.382	73.51	69.6
16	0.544	0.495	0.489	66.54	62.2

considered for the purpose of comparison with air core diameter predicted from the present model. Tables 1a–d show such comparisons where the air core diameters, d_a, have been calculated from the empirical values of liquid film thickness as $d_a = d_o - 2t_f$. Though the comparisons show the identical qualitative trends for the variation of air core diameter with nozzle geometry in all the cases, the quantitative predictions of air core diameter from the present work do not conform the empirical results and always show relatively lower values. Apart from the limitations of the present theory in using the standard k-ε turbulence model with the logarithmic law of the wall in case of a strongly swirling flow, the important fact, which can probably describe the above discrepancy is that, the determination of air core diameter inside the nozzle from the measured value of liquid film thickness at discharge orifice is not justified since a little enlargement in the size of the air core takes place near the exit plane of the orifice in practice (as shown in Fig. 1b). Therefore, the air core diameter determined from the liquid film thickness at the discharge plane of the orifice ($d_a = d_o - 2t_f$) will usually overestimate the uniform diameter of air core inside the nozzle predicted by any theory. This is corroborated further by the fact that the air core diameter, determined from the empirical results of liquid film thickness (Suyari and Lefebvre, 1986) at nozzle orifice, even exceeds, under all situations, the value given by the inviscid flow theory of Taylor (1948) (Tables 1a–d). However, in practice, as the viscous effects diminish the swirling intensity of the flow, the actual air core diameter should have been lower than that predicted by the inviscid theory.

Comparisons of the values of coefficient of discharge predicted by the present model with the empirical values of Rizk and Lefebvre (1985a) and Jones (1982) are shown in Tables 2a–d, while such comparisons for spray cone angle with the empirical values of Rizk and Lefebvre (1985b) are also shown in Tables 2a–d. The present model predicts the similar qualitative trends for the variations of C_d and ψ with the geometrical dimensions of the nozzle as furnished by empirical information in practice. The present theory overestimates the values of coefficient of discharge as compared to those furnished by empirical results, the difference being within 5–20%. The predicted values of spray cone angle from the present model agree fairly well with the empirical values under all situation except for the cases of orifice diameters of 1.5 and 1.0 mm. It is a fact that the spray cone angle decreases considerably in practice with a decrease in orifice diameter for a given flow rate through the nozzle as depicted by the result of the present model. However, the discrepancy in the results of the present predictions with the empirical values of Rizk and Lefebvre (1985b) may probably be attributed to the uncertainties in the use of the empirical equation provided by them in the range associated with the operating variables at orifice diameter of 1.5 and 1.0 mm.

5. Conclusion

Theoretical predictions of air core diameter, coefficient of discharge and spray cone angle of a simplex type swirl spray pressure nozzle have been made from the numerical computation of flow within the nozzle. The diameter of the central air core inside the nozzle has been predicted as the one beyond which the resistance to the flow in the nozzle increases rapidly at a given operating condition.

- With an increase in the nozzle flow rate at its lower range there occurs a sharp increase in the air core diameter and spray cone angle, but a sharp decrease in the coefficient of discharge. However, all the parameters become independent of the flow rate at its higher range.
- An increase in either the orifice diameter or the swirl chamber cone angle, or a decrease in the area of the inlet tangential ports increases the air core diameter and spray cone angle while decreases the coefficient of discharge.
- The theoretical prediction of a uniform air core diameter in the nozzle does not conform with that determined from the empirical results of liquid film thickness at the discharge orifice. The theoretical predictions of coefficient of discharge and spray cone angle agree well with the available empirical information although the theoretically predicted values are little higher than the actual ones.

References

Binnie, A.M., Harris, D.P., 1950. The application of boundary layer theory to swirling flow through a nozzle. Quart. J. Mech. and Appl. Math. 3, 89.

Binnie, A.M., 1955. Viscosity effects in the nozzle of a swirl atomizer. Quart. J. Mech. and Appl. Math. 8, 394.

Binnie, A.M., Teare, J.D., 1956. Experiments in the flow of a swirling water through a pressure nozzle and an open trumpet. Proc. Roy. Soc. London A 235, 78.

Binnie, A.M., Hakings, G.A., Kamel, M.Y.M., 1957. The flow of swirling water through a convergent–divergent nozzle. J. Fluid Mech. 3, 261.

Chen, S.K., Lefebvre, A.H., Rollbuhler, J., 1992. Factors influencing the effective spray cone angle of pressure swirl atomizers. ASME J. Engrg. Gas Turbine and Power 114, 97.

Giffen, E., Massey, B.S., 1950. Some observations on flow in spray nozzles. Motor Industry Res. Assoc. Report No. 1948/4.

Harlow, F.H., Welch, J.E., 1965. Numerical computation of time-dependant viscous incompressible flow of fluid with a free surface. Phys. Fluid 8 (12), 2182.

Hirt, C.W., Cook, J.L., 1972. Calculating three-dimensional flows around structures and over round terrain. J. Comp. Phys. 10, 324.

Jones, A.R., 1982. Design optimization of a large pressure jet atomizer for power plant. In: Proceedings of the Second International Conference on Liquid Atomization and Spray Systems, p. 181.

Kutty, S.P., Narasimhan, M., Narayanaswamy, K., 1978. Design and prediction of discharge rate, cone angle and air core diameter of swirl chamber atomizers. In: Proceedings of the First International Conference on Liquid Atomization and Spray Systems, p. 93.

Rizk, N.K., Lefebvre, A.H., 1985a. Internal flow characteristics of simplex swirl atomizers. AIAA J. Propul. and Power 1 (3), 193.

Rizk, N.K., Lefebvre, A.H., 1985b. Prediction of velocity coefficient and spray cone angle for simplex swirl atomizers. In: Proceedings of the Third International Conference on Liquid Atomization and Spray Systems, p. 111c/2/1.

Som, S.K., Mukherjee, S.G., 1980. Theoretical and experimental investigations on the formation of air core in a swirl spray atomizing nozzle. Appl. Scientific Res. 36, 173.

Suyari, M., Lefebvre, A.H., 1986. Film thickness measurements in a simplex swirl atomizers. AIAA J. Propul. and Power 2 (6), 528.

Tate, R.W., Marshall, W.R., 1953. Atomization by centrifugal nozzles. J. Chem. Engrg. Prog. 49, 169.

Taylor, G.I., 1948. The mechanics of swirl atomizers. In: Proceedings of the Seventh International Congress for Applied Mechanics. 2 (1), p. 280.

Taylor, G.I., 1950. The boundary layer in the converging nozzle of a swirl atomizer. Quart. J. Mech. and Appl. Math. 3, 129.

Wang, X.F., Lefebvre, A.H., 1987. Influence of ambient air pressure on pressure swirl atomization. Atomization and Spray Tech. 3, 209.